Theoretical model for ultracold molecule formation via adaptive feedback control

Ulrich Poschinger[1]**, Wenzel Salzmann**[1]**, Roland Wester**[1]**, Matthias Weidemüller**[1]**, Christiane P Koch**[2,3] **and Ronnie Kosloff**[2]

[1] Physikalisches Institut der Universität Freiburg, Hermann-Herder-Str. 3, 79104 Freiburg, Germany
[2] Department of Physical Chemistry and The Fritz Haber Research Center, The Hebrew University, Jerusalem 91904, Israel

E-mail: roland.wester@physik.uni-freiburg.de, m.weidemueller@physik.uni-freiburg.de and ckoch@physik.fu-berlin.de

Abstract

We theoretically investigate pump-dump photoassociation of ultracold molecules with amplitude- and phase-modulated femtosecond laser pulses. For this purpose, a perturbative model for light-matter interaction is developed and combined with a genetic algorithm for adaptive feedback control of the laser pulse shapes. The model is applied to the formation of $^{85}Rb_2$ molecules in a magneto-optical trap. We find that optimized pulse shapes may maximize the formation of ground state molecules in a specific vibrational state at a pump-dump delay time for which unshaped pulses lead to a minimum of the formation rate. Compared to the maximum formation rate obtained for unshaped pulses at the optimum pump-dump delay, the optimized pulses lead to a significant improvement of about 40% for the target level population. Since our model yields the spectral amplitudes and phases of the optimized pulses, the results are directly applicable in pulse shaping experiments.

(Some figures in this article are in colour only in the electronic version)

1. Introduction

One of the challenges in contemporary atomic and molecular physics is the making of ultracold molecular samples [1–3]. Direct cooling techniques for molecules have not yet reached the ultracold regime ($T < 1$ mK). Instead, ultracold atoms are assembled to molecules using magnetic Feshbach resonances [4] or photoassociation [5, 6]. In the latter case, typically a continuous-wave (cw) laser excites a pair of colliding atoms into a long-range molecular state. Subsequent spontaneous emission leads to molecules in their electronic ground state. In view of prospective applications, stable ultracold molecules, i.e. molecules

---

[3] Present address: Institut für Theoretische Physik, Arnimallee 14, 1495 Berlin, Germany.
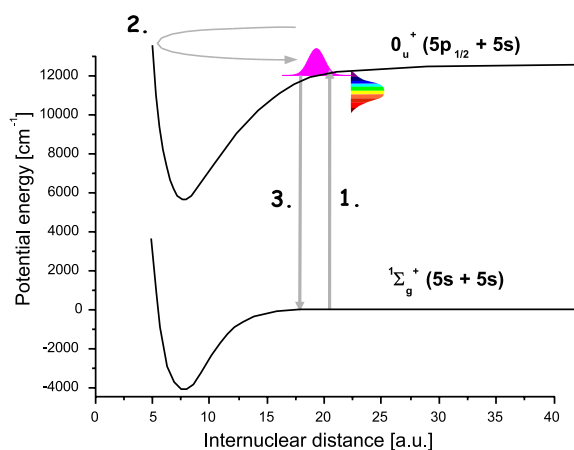
Figure 1. The pump-dump scheme for the production of ultracold molecules with short laser pulses. A wavepacket is created in the excited state by a pump pulse (1) and subsequently propagates (2). A dump pulse transfers population to the target bound ground state level after a suitable time delay (3).

in their absolute rotational, vibrational and electronic ground states are required. However, molecules formed with Feshbach resonances are created in the highest bound vibrational level [4]. Photoassociation with a cw laser followed by spontaneous emission forms molecules in a range of vibrational levels [7]. In this case, the radiative lifetime of the excited electronic state ultimately represents the rate-determining step in ground state molecule formation. When applied to a Bose–Einstein condensate (BEC), the incoherent nature of the spontaneous decay furthermore destroys the coherence of the BEC and hence the condensate itself [8]. This may be avoided by stimulated Raman transitions [9]. Recently, light-driven Rabi oscillations between atoms and molecules have also been observed [10]. Using cw photoassociation in combination with nanosecond-pulsed Raman transitions, the formation of RbCs molecules in the $v = 0$ level of the ground electronic state has been achieved [11].

An alternative approach to ultracold molecule formation is the photoassociation with time-dependent laser fields of femtosecond to picosecond pulse durations. The conceptually simplest pulsed photoassociation scheme is based on a two-pulse pump-dump population transfer from the atomic continuum to a bound molecular level [12], as shown in figure 1. The pump pulse excites a molecular wavepacket of the vibrational states within its bandwidth, which then propagates until it is dumped to the ground state by a second laser pulse. By modifying the delay time between the two pulses, the transition to one or several desired target vibrational levels in the ground state can be enhanced by quantum interference. Here, the production rate is not limited by the radiative lifetime of the intermediate state, but by the much shorter vibrational period, by the Franck–Condon factors and ultimately by the unitarity limit of the scattering rate [8, 13]. The particular advantage of this approach is that the pump-dump delay time and the pulse shapes yield additional control knobs to prepare specific product states, which is extensively explored in the field of adaptive feedback control with shaped femtosecond pulses [14, 15]. A number of theoretical studies have investigated the use of chirped laser pulses for excitation [16–18] and stabilization [19, 20] of ultracold molecules. Even larger control over the molecule formation process might be obtained by shaped laser pulses. Laser pulses which optimize the formation of ultracold molecules from an atomic BEC have been calculated using the optimal control theory [21]. In many cases, the complexity of

the pulse shapes resulting from optimal control calculations requires a careful transformation into experimentally achievable pulse shapes [22, 23].

In this paper, adaptive feedback control of photoassociation with femtosecond laser pulses is investigated theoretically. For this purpose, the properties of typical femtosecond oscillator pulses and a realistic pulse shaping device are combined with a closed-loop genetic algorithm for pulse shape optimization. The resulting pulse shapes are obtained as amplitudes and phases in the frequency domain, similar to the case in closed-loop adaptive feedback control experiments. The parameters of the calculations are chosen to correspond to a situation, which is typical for state-of-the-art experiments [24]. A two-channel model is employed, which simplifies the complex coupled-channel dynamics, but retains the important features of pump-dump photoassociation. The goal of this study is to qualitatively determine to which extent the formation process of ground state molecules can be controlled by realistic shaped laser pulses.

The first experiment on photoassociation with femtosecond laser pulses has been carried out on hot mercury atoms [25]. In the ultracold regime, electronically excited Na_2 molecules have been formed using picosecond pulses near-resonant to the sodium D1 transition and probed with a subsequent laser pulse [26]. Chirped nanosecond laser fields have been employed to enhance inelastic collision rates in an ultracold gas [27]. Also, the effect of the chirp of femtosecond pulses on the dissociation of ultracold Rb_2 molecules has been investigated [28]. Recently, adaptive feedback control with shaped femtosecond pulses has been applied in our group to optimize the dissociation of ultracold Rb_2 molecules from a magneto-optical trap [24]. We envision that the work presented in this paper will be helpful for the first experimental demonstration of ultracold ground state molecule formation using pulsed photoassociation, which has not been achieved to date.

The paper is organized as follows: the model of two colliding atoms interacting with the laser fields is described in section 2.1. A perturbative treatment of the interaction with the field is employed in section 2.2 to obtain a model for the pulse shaping device. Its optimization with a genetic algorithm is outlined in section 2.3. The results are presented in section 3. The validity of the perturbative model is tested in section 3.1 by a comparison to full, non-perturbative quantum calculations. In section 3.2 and 3.3 the results for optimal laser pulses for pulsed photoassociation, as obtained from adaptive feedback control, are presented and analysed.

2. Model for the photoassociation process

2.1. Interaction of two colliding atoms with a laser field

A colliding atom pair subject to a laser pulse is considered. Two electronic states coupled by the radiation field are taken into account with the assumption of the rotating wave approximation. The centre-of-mass motion of the two atoms is assumed to be decoupled from the internuclear dynamics. The time-dependent Schrödinger equation then reads

$$i\hbar \frac{\partial}{\partial t} \begin{pmatrix} \psi_g(R,t) \\ \psi_e(R,t) \end{pmatrix} = \hat{H} \begin{pmatrix} \psi_g(R,t) \\ \psi_e(R,t) \end{pmatrix}, \tag{1}$$

with

$$\hat{H} = \begin{pmatrix} \hat{T} + V_g(R) & \hbar\Omega(t) \\ \hbar\Omega^*(t) & \hat{T} + V_e(R) - \Delta \end{pmatrix}. \tag{2}$$

The wavefunction consists of one component for the ground state, $\psi_g(R,t)$, and one component for the excited state, $\psi_e(R,t)$. The diagonal elements of the Hamiltonian are

given by the kinetic energy operator $\hat{T}$ and the potential energy curves for the respective states $V_{g/e}(R)$ which depend on the internuclear separation R. The zero of energy is chosen to correspond to the ground state dissociation limit. Within the rotating wave approximation, V_e is shifted by the detuning Δ with respect to V_g where $\Delta = \hbar(\omega_{ge} - \omega_L)$. ω_{ge} denotes the atomic transition frequency and ω_L denotes the carrier frequency of the laser. The off-diagonal elements of the Hamiltonian are given by the complex time-dependent Rabi frequency $\Omega(t)$, which is related to the electric field $\tilde{\mathcal{E}}(t)$ by $\Omega(t) = \mu\tilde{\mathcal{E}}(t)/\hbar$. Here, μ denotes the dipole matrix element of the two molecular electronic states under consideration. In the following, the R-dependence of this matrix element is neglected and its asymptotic value is employed, $\mu = 2.537 \times 10^{-9}$ cm for the Rb D1 line. The laser pulse is assumed to be derived from a Gaussian transform-limited pulse sent through a pulse shaping device as detailed in section 2.3.

The two channels under consideration for the calculations are the singlet ground state $X^1\Sigma_g(5s + 5s)$ and the excited state $0_u^+(5s + 5p_{1/2})$ of ^{85}Rb$_2$. The wavelength of the asymptotic (atomic) transition corresponds to 794.9 nm. The potential energy curves are derived from *ab initio* data [29] at short distances and long-range dispersion potentials $(-C_3/R^3) - C_6/R^6 - C_8/R^8$ for distances larger than the LeRoy–Bernstein radius. The coefficients for the 5s + 5s asymptote are found in [30], while the coefficients for the 5s + 5p asymptote are taken from [31]. Hund's case (c) representation of the potential energy curves is obtained by diagonalizing Hund's case (a) potentials coupled by spin–orbit interaction [32]. The spin–orbit coupling matrix element is set to the atomic value. The R-dependence and the resonant character of the spin–orbit coupling are neglected. The latter leads to strong perturbations in the vibrational spectrum [33] providing an efficient stabilization mechanism for pump-dump photoassociation [20]. However, its treatment would require a three-channel model, and the focus of this study is on the qualitative understanding of possible control over the wavepacket dynamics.

Hamiltonian equation (2) is represented on a grid using the mapped Fourier grid method [34, 35]. A grid of 1024 points extending up to 27 000 Bohr radii is chosen. This size is necessary to obtain a reliable representation of continuum scattering states [18]. The binding energies $E_v^{g/e}$ and wavefunctions $\varphi_v^{g/e}(R)$ of the vibrational levels are computed by diagonalizing Hamiltonian equation (2) with $\Omega(t) = 0$. The Franck–Condon factors are then obtained as scalar products, $|\langle v|w\rangle|^2 = \int dR \left|\varphi_v^e(R)^*\varphi_w^g(R)\right|^2$. To test the validity of the perturbative model which is explained in the following section, the time-dependent Schrödinger equation (1) is solved with the Chebyshev propagator method [36].

The initial state of the colliding atom pair is chosen such as to describe an ultracold atomic gas in a magneto-optical trap. Due to the low temperatures of about 100 μK, only a narrow band of continuum states above the ground state potential asymptote is occupied. The considerations in this study focus on a single initial continuum state with collisional angular momentum $l = 0$, i.e. an s-wave scattering state. This assumption is justified since the continuum wavefunctions corresponding to temperatures $\leqslant 500$ μK possess an identical nodal structure at short and intermediate internuclear distances. A thermal average over all possible initial states is only required for absolute molecule formation rates, which is beyond the scope of the present study.

2.2. Model of the photoassociation process with shaped laser pulses

In the following, a perturbative model of pump-dump photoassociation with arbitrarily phase- and amplitude-modulated laser pulses is presented. Such shaped laser pulses are prepared experimentally by passing the spectrally dispersed pulses through a liquid crystal modulator

array. In each pixel of such a pulse shaper, the phase and the amplitude of the corresponding frequency component of the pulse can be computer controlled.

The photoassociation pulse creates a time-dependent wavepacket in the excited state. After the pulse is off, the excited state wavefunction $\psi_e(R; t)$ is given by a superposition of vibrational levels in the excited state. If the interaction can be treated perturbatively, i.e. the Rabi angle, $\theta = \int \Omega(t)\, dt$, is small compared to π, the pulse excites the superposition of vibrational levels given by [37]

$$\psi_e(R; t) \propto \sum_v a_v \mathcal{E}(\omega_v)\langle v|E\rangle \varphi_v(R)\, e^{-iE_v^e t/\hbar}, \tag{3}$$

where $\langle v|E\rangle$ is the overlap integral of the initial continuum state $|E\rangle$ and the excited state vibrational level v; its square corresponds to the free-bound Franck–Condon factors. The frequency spectrum of the electric field of the laser pulse, $\mathcal{E}(\omega)$, is evaluated at the transition frequency ω_v to the vibrational level v. The a_v coefficients are introduced to represent the complex modulation coefficients of a pulse shaper. This description assumes that the frequency components for each contributing v are individually resolved by the pulse shaper. As one can experimentally only diminish spectral components, one obtains the constraint $0 \leqslant |a_v| \leqslant 1$. Equation (3) is only valid if the pulse does not contain significant amplitude at frequencies close to resonance with the atomic transition. This is due to the strongly increasing transition strength close to the atomic resonance, which leads to a breakdown of the perturbative treatment for typical laser intensities. We estimate that the perturbative model is valid if the detuning of the laser pulse spectrum with respect to the atomic transition is large enough so that minimal excitation of the atomic transition occurs. After a delay time Δt, a second or dump pulse $\mathcal{E}'(\omega)$ is applied. This pulse transfers population from the excited state to the ground state; it is assumed not to be shaped by a pulse shaper. The resulting superposition of *bound* ground state levels reads

$$\psi_g^{\text{bound}}(R; t) \propto \sum_{v,w} a_v \mathcal{E}(\omega_v)\mathcal{E}'(\omega_{vw})\langle E|v\rangle\langle v|w\rangle \varphi_w(R)\, e^{-\frac{i}{\hbar}E_w^g(t-\Delta t)}\, e^{-\frac{i}{\hbar}E_v^e\Delta t}. \tag{4}$$

Note that this description is only valid for non-overlapping pulses because transient dynamics that occur during the excitation process are not included. Therefore, only delay times Δt that are large compared to the duration of the pump and dump pulses are chosen. In equation (4), v runs over all bound vibrational levels of the excited electronic state and w over all bound levels of the ground state. $\langle v|w\rangle$ are overlap integrals between ground and excited state bound levels. The time delay between the two pulses enters the expression through the phase factors $e^{-iE_v^e\Delta t/\hbar}$ which corresponds to the propagation of the wavepacket in the excited state. The population of an individual bound ground state level w is now given by

$$|b_w|^2 = \sum_{v,v'} a_v a_{v'}^* \mathcal{E}(\omega_v)\mathcal{E}'(\omega_{vw})\mathcal{E}^*(\omega_{v'})\mathcal{E}'^*(\omega_{v'w})\,\langle E|v\rangle\langle v|w\rangle\langle w|v'\rangle\langle v'|E\rangle\, e^{-\frac{i}{\hbar}(E_v^e - E_{v'}^e)\Delta t}. \tag{5}$$

This double sum over the excited state vibrational levels v and v' can be concisely written as a complex quadratic form in terms of the pulse modulation coefficients a_v,

$$|b_w|^2 = \sum_{v,v'} a_{v'}^* M_w^{vv'}(\Delta t)a_v. \tag{6}$$

The Franck–Condon matrix $M_w^{vv'}(\Delta t)$ contains the properties of the system (overlap integrals and binding energies) and of the frequency spectrum of the two laser pulses and their pulse delay.

It can be inferred from equation (6) that the choice of modulating the pump pulse and not the dump pulse is in fact arbitrary since the same structure of equation (6) is obtained if the dump pulse or both pulses are shaped. Equation (6) serves two purposes. First, for a given target level w, it can be used to obtain the optimal detuning of the pulses by evaluating $|b_w|^2$ for different delay times Δt. Second, it allows for the implementation of an optimization procedure as explained in the following section.

2.3. Genetic algorithm for the pulse optimization

In the following, the photoassociation pulse shall be optimized while the dump pulse is assumed to be transform limited. An optimization algorithm is obtained by combining the analysis of the target state equation (6) with a spectral decomposition of the pulse. The photoassociation pulse which yields the desired excited state wavepacket can, in principle, be spectrally composed from a set of weighted delta functions at the transition frequencies corresponding to the vibrational states v [37]. This spectrum of a few sharp structures leads to very long pulses in a time domain, which is unfavourable for our perturbative model of a pump-dump scheme as explained above. The photoassociation pulse is instead constructed from a coherent superposition of a larger number of frequency components,

$$\hbar \Omega(t) = \mu \sum_{n=1}^{N_p} c_n \mathcal{E}(\omega_n) \, e^{i(\omega_n - \omega_L)t}, \tag{7}$$

which leads to a shorter pulse in the time domain. The frequency spectrum of the pump and dump laser pulses before modifications by the pulse shaper is assumed to be a Fourier-limited Gaussian pulse $\mathcal{E}(\omega_n) \propto \exp[-(\omega_n - \omega_L)^2/2\Gamma^2]$ with a root-mean-square width Γ. Each ω_n corresponds to a pixel in the pulse shaper mask; ω_L is again the carrier frequency of the laser pulse. The pixel number N_p is set to 640 and the frequency spacing from pixel to pixel is set to 1.5 cm^{-1}, which are numbers used in experimentally available pulse shaping devices. This leads to a pulse shaper resolution that is smaller than the vibrational level spacing for almost all the excited vibrational levels. The pulse shaper coefficients c_n are set equal to the desired superposition coefficients a_v from equation (6), where v is the excited state level for which $\hbar E_v$ is closest to ω_n. The range of vibrational levels which contribute to the population in the excited state is identified by the non-vanishing matrix elements of $M_w^{vv'}$. In the present case, this range consists of 150 levels ranging from $v = 170$ ($T_{\text{vib}} = 0.77$ ps) to $v = 320$ ($T_{\text{vib}} = 80.0$ ps). The discreteness of the spectrum, equation (7), still leads to unwanted replica effects in the time domain. The pulse is therefore multiplied with a box function of the form $\exp[-(t/T_{\text{cutoff}})^m]$ with $m = 8$ and $T_{\text{cutoff}} = 3.33$ ps; t is the time relative to the maximum of the pulse envelope. This provides a smooth switching on and off of the pulse.

The optimization is carried out with respect to a_v in equation (6), corresponding to the pixels of a pulse shaping device. The pump-dump delay time Δt represents a fixed parameter for the optimization process. It turns out that for the amplitude optimization, it is sufficient to set a_v to either 0 or 1. For the phase, 256 possible values are considered, leading to an overall 9 bit optimization of a_v. The quality of the pulses is determined by the fitness factor Q which is chosen as

$$Q = \frac{|b_w|^2}{\sqrt{\langle t^2 \rangle}}. \tag{8}$$

Here, $\langle t^2 \rangle$ is a measure of the pulse duration:

$$\langle t^2 \rangle = \frac{\int t^2 \Omega(t) \, dt}{\int \Omega(t) \, dt}. \tag{9}$$
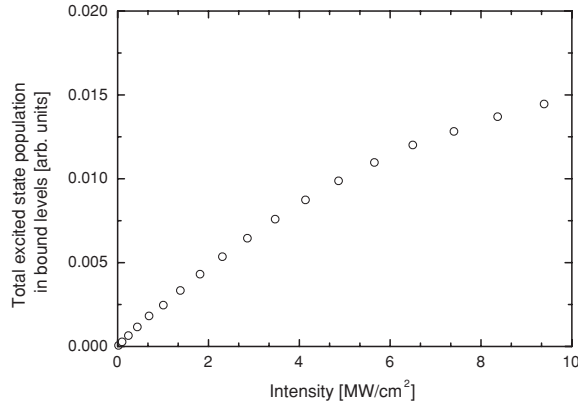
Figure 2. Dependence of the excitation probability on the peak intensity of the pump pulse for a fixed pulse width of 100 fs FWHM. The linear dependence on intensity below 2 MW cm^{-2} shows the validity of a perturbative treatment.

It is included in the definition of the fitness factor in order to keep the pulses as short as possible. This is not a physical constraint but a requirement of the perturbative model because the duration of the pulses is immensely increased by the modulation. Already, a linear frequency chirp stretches the pulse in time. The employed perturbative model, however, requires non-overlapping pump and dump pulses, as explained above.

The optimization of the formation of molecules in a specific ground state level w is carried out by means of an evolutionary algorithm. This corresponds directly to a close-loop experiment. For the calculations a very basic evolutionary algorithm, *SimpleGA* from the *GALib* package [38], is employed. Populations of 20 individuals are used, and the number of generations is set to 1000. This is sufficient to obtain convergent results. The single-bit mutation and single-bit crossover probabilities are chosen as 0.005 and 0.8, respectively.
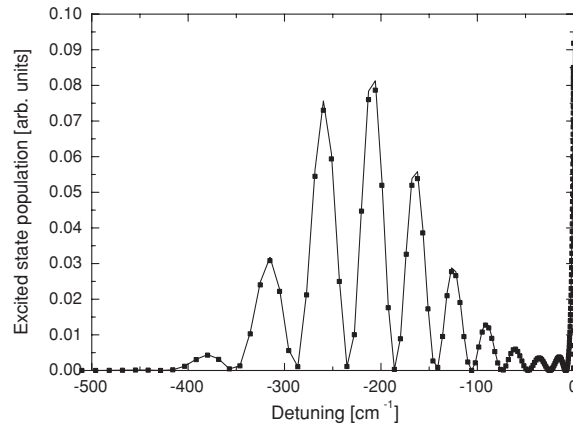
3. Results

3.1. Validity of the pulse shaper model

The pulse shaper model of equation (6) is derived for the case of a small perturbation of the atom pair by the laser field. Higher order processes, in particular Rabi cycling during the pump or dump pulse, are neglected. By carrying out calculations for a single unshaped pump pulse with varying peak intensity of the pulse, the regime of validity of the perturbative approximation is analysed.

In figure 2 the probability of exciting an atom pair to the excited state is shown as a function of the pulse's peak intensity. These results are obtained by solving the time-dependent Schrödinger equation where the field is treated non-perturbatively. Figure 2 clearly shows a linear dependence of the excitation probability for small intensities $<4 \times 10^6$ W cm^{-2}. For these low intensities, the effect of the laser field can be treated in a first-order perturbation theory. For larger pulse energies, excitation starts to saturate, which indicates the transition to a non-perturbative regime. This is attributed to Rabi cycling and strong off-resonant excitations.

In order to check the validity of equation (6) in the perturbative regime, a model study is performed. The excitation of a vibrational wavepacket in the excited state, $\psi_e(R; t)$, is calculated with equation (3) for a single Fourier-limited Gaussian pump pulse. The detuning

Figure 3. A comparison between the predicted excited state level populations after the pump pulse from the model (solid line) and the results of the quantum dynamical calculation (squares).

of the pulse is set to $\Delta = 251$ cm^{-1} and the temporal intensity width to 100 fs FWHM. These values match the experimental conditions of [24]. In figure 3, the projections of the excited state wavepacket onto the excited vibrational eigenfunctions $\varphi_v^e(R)$ are shown as a function of the detuning, E_v^e (solid line). This is compared in figure 3 to the non-perturbative calculation for the same pulse parameters (squares). A good agreement of the projections is observed in the range of resonant levels.

As described above, the perturbative pump–dump model is only valid for non-overlapping pulses because transient dynamics occurring during the pulsed excitation are not included. Therefore, in a second step it is checked if equation (6) holds for two-pulse pump–dump processes. Assuming two pulses with width and detuning, as given above, the pump–dump process is calculated with equation (5) for varying delay time. This yields the ground state wavepacket which is then projected onto a single target vibrational level. The level $w = 119$, bound by $E_{119}^g = 6.86$ cm^{-1}, is selected because it features a large Franck–Condon factor from the excited state vibrational levels that are populated at the given detuning of the laser pulse (see section 3.2 and figure 5). The population in this target level is shown in figure 4 (solid line) as a function of the pump–dump delay time. It is compared to the results obtained by solving the time-dependent Schrödinger equation (squares). The agreement between the perturbative model and the full quantum dynamics with a non-perturbative treatment of the field is convincing.

Note that in the present case, the optimal pump–dump delay is given by the full excited state wavepacket round-trip time T_{vib} and integer multiples thereof. According to the Franck–Condon principle, this indicates that the dump transition occurs at the outer turning point of the excited state wavepacket, as indicated in figure 1. This is not necessarily the case since it depends strongly on the molecular potential curves and the laser detuning. The dump transition will occur at half-integer multiples of T_{vib}, corresponding to the inner turning point if the potential facilitates a deceleration mechanism at short distances. This is the case for a soft repulsive wall such as in the outer well of the $0_g^-(p_{3/2})$ state [19], or for resonant coupling [20].

3.2. Optimal detuning

In order to find a window of detunings suitable to populate target levels in the ground state, equation (6) is evaluated for unshaped Fourier-limited Gaussian pulses of 100 fs FWHM
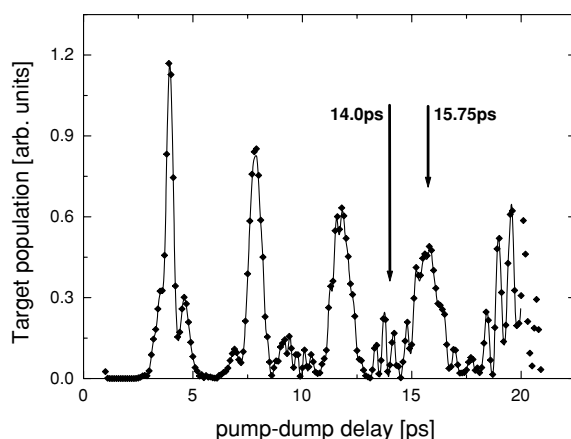
Figure 4. Target state population $|b_w|^2$ for $w = 119$ from equation (6) (solid line) compared to the results of the quantum dynamical calculation (squares). The peaks are closely connected to the wavepacket dynamics in the excited state potential well. The temporal smearing out of peak heights is due to anharmonic dispersion of the wavepacket.
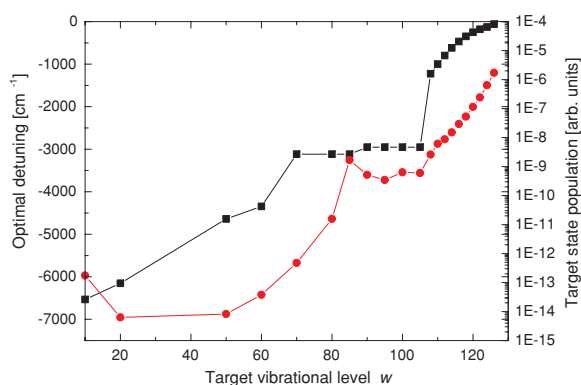
Figure 5. Optimal detuning (black ■, left axis) for pump–dump photoassociation with two identical unshaped femtosecond laser pulses, estimated from equation (6) for a range of target vibrational levels w in the ground state. The maximum attainable population of these levels (red ●) is shown on the right axis.

intensity width. For a range of delay times encompassing several round-trip times, the Franck–Condon matrix $M_w^{vv'}(\Delta t)$ is calculated for each ground state target level w. The optimal detuning is inferred from the maximum of the main diagonal of $M_w^{vv'}(\Delta t)$ and the corresponding maximum target state population is calculated. Figure 5 shows the result for both the optimal detuning and corresponding target state population as a function of the vibrational level w of the ground electronic state. A strong dependence of the maximum attainable population on the vibrational level is observed spanning eight orders of magnitude. The largest target populations are found for small laser detunings and correspond to high target vibrational levels. This reflects the large free–bound Franck–Condon factors for highly excited vibrational levels. It also shows that the bound–bound Franck–Condon factors for the dump step favour high target levels for small detunings.
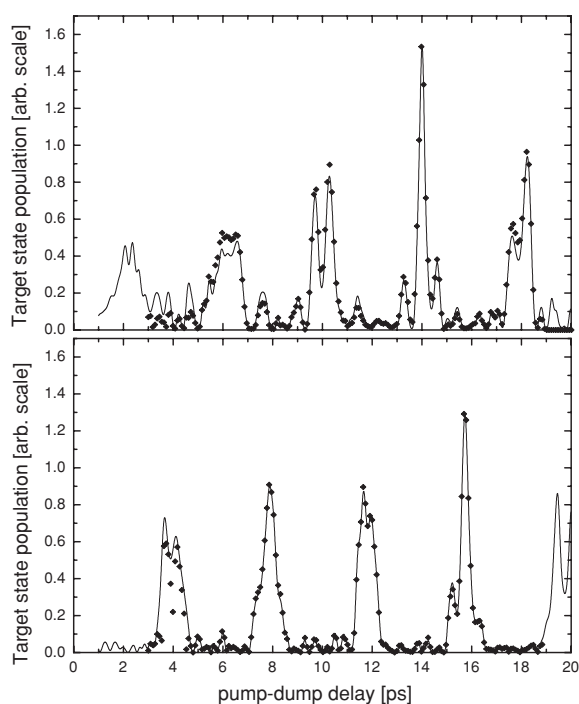
Figure 6. Relative target state ($w = 119$) population versus pump-dump delay for optimized pump pulses. The target level population on the vertical axis of the graphs is given in the same units as in figure 4 and can thus directly be compared. The optimizations are carried out with a delay parameter of 14.00 ps (upper trace) and 15.75 ps (lower trace), corresponding to a minimum and a maximum in the 'natural' dynamics after an unshaped pump pulse (cf figure 4). The pulse parameters are the same as in figure 3. The prediction of the model equation (6) (solid line) is compared to the solution of the time-dependent Schrödinger equation (squares). Note the deviations occurring at small delay times which are due to transient excitations.

3.3. Adaptive feedback control

With the perturbative model, optimization calculations are carried out for pump-dump photoassociation. As in the previous section, the pump and dump pulses are assumed to be Fourier-limited Gaussian pulses with 100 fs FWHM intensity width and $\Delta = 251$ cm^{-1} detuning. The goal for the optimization is to find the pump pulse that maximizes the population in the $w = 119$ ground state vibrational level, which is a suitable level for the chosen detuning due to its large Franck–Condon overlap (see section 3.1). The spectral components of the pump pulse are optimized with respect to their phase and amplitude. The pump-dump delay time, which represents a parameter in these calculations, is set either to 15.75 ps or to 14.0 ps. As shown in figure 4, for $\Delta t = 15.75$ ps a maximum is observed in the target level population of the 'natural' dynamics, i.e. the dynamics obtained with an unshaped pump pulse. On the other hand, $\Delta t = 14.0$ ps represents a delay for which the natural dynamics leads to almost no-target level population.

The resulting target state population with optimized phases and amplitudes is shown as a function of the pump-dump delay time in figure 6 (solid lines). Note that the target level population on the vertical axis of both graphs in figure 6 and of the graph in figure 4 is given in same units and can thus directly be compared. In figure 6, it is clearly seen that for both optimization calculations the maximum population is indeed obtained at the delay time for
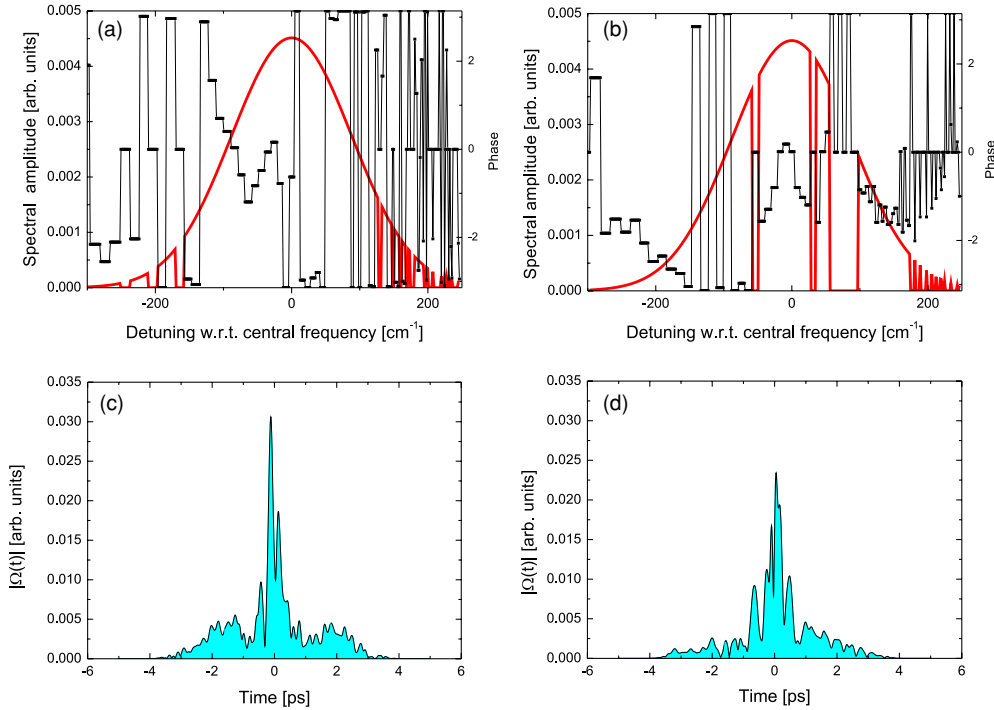
Figure 7. Upper panels: amplitude (red ——) and phase (black ······) mask patterns of the pulse shaper to generate the optimized pulses for $\Delta t = 14.00\,ps$ (a) and $\Delta t = 15.75$ ps (b). The amplitudes are multiplied by the spectral envelope of the pulse. Note the chirp-like structures in the phases of the two pulses. Lower panels: temporal amplitude of the optimized pulses for the 14.00 ps case (c) and the 15.75 ps case (d).

which the pump pulse is optimized. For $\Delta t = 14.00$ ps, the dynamics is modulated such that an efficient dump transition may occur at delay times when almost no-target level population is obtained with an unshaped pump pulse (see the left arrow in figure 4). In this case, the target level population for the optimized pulse amounts to 1.6 arb. units, whereas less than 0.1 arb. units are observed for the same pump-dump delay with an unshaped pulse, corresponding to an increase by more than a factor of 10. This illustrates that the pulse shaper can be used to a great extent to control the wavepacket dynamics. The optimal pulse shapes also lead to a higher maximum of the target level population as compared to the maximum population achieved for the optimal pump-dump delay time with unshaped pulses; for the optimization at $\Delta t = 14.0$ ps, the target population is enhanced by about 40%. For 15.75 ps a smaller enhancement of about 10% is observed. The two different levels of optimization are attributed to the different integrated energies of the obtained optimal pulse, as detailed below.

The results of the optimization are compared with the results of the time-dependent Schrödinger equation using the optimal pulses, obtained above, as pump pulses. The time delay between the pump and dump pulses is varied to investigate whether the optimal result is indeed obtained for the intended delay and how in general the pulse shapes affect the excited state wavepacket dynamics. As shown in figure 6, these results agree well with the model except for very short delay times where the pulses still overlap.

The mask patterns of the pulse shaper for amplitude (——) and phase (······) are shown for the two preset delay times in the top panels (a) and (b) of figure 7. The spectrum contains
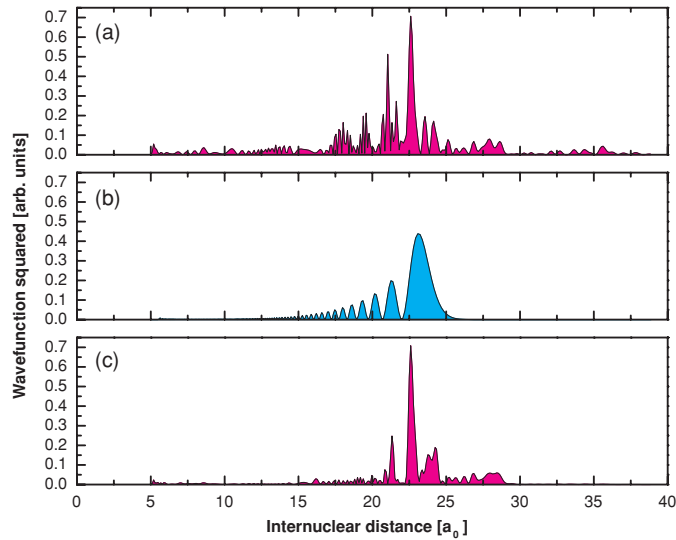
Figure 8. Excited state wavepackets in a position space at $t = 15.75$ ps after the pump pulse maximum. The upper panel (a) shows the wavepacket obtained after an unshaped pulse, while the lower (c) panel displays the wavepacket resulting from excitation with a pulse optimized for $\Delta t = 15.75$ ps. To estimate the dump efficiency, these wavepackets have to be compared to the stationary ground state wavefunction of the target level shown in the middle panel (b). Note the reduced probability density at small internuclear distances of the wavepacket after the optimized pulse as compared to the unshaped case.

frequencies for which the excited state levels $v = 204$ to $v = 249$ are resonantly excited from the initial state. For $\Delta t = 14.0$ ps, figure 7(a), almost the full spectrum is retained, whereas for $\Delta t = 15.75$ ps, figure 7(b), some frequency components are removed from the pulse spectrum. This leads to a smaller integrated energy of the optimized pulses for the $\Delta t = 15.75$ ps optimum. Therefore, a smaller target level population is observed on the maximum (about 1.3 arb. units) for the 15.75 ps calculation as compared to the 14.0 ps calculation (1.6 arb. units). Chirp-like structures in the spectral phase emerge in both cases. In other runs of the optimization algorithm, such structures have been obtained as well.

The temporal profiles of the optimized pulses are shown in the bottom panels (c) and (d) of figure 7. The pulses are stretched in time compared to the time duration of the unshaped pulses of 100 fs FWHM. For $\Delta t = 14.0$ ps, figure 7(c), three sub-pulses are observed which are separated by about 2 ps. This has to be compared to the vibrational times of the excited state levels which range from 2.7 ps for $v = 204$ to 10.0 ps for $v = 249$ and 4 ps for the central level $v = 219$ resonant with the carrier frequency. In the Wigner representation of the optimal field (data not shown), an interference pattern between the three sub-pulses is observed indicating the intricate phase relation between the sub-pulses. The 'holes' in the spectrum observed for $\Delta t = 15.75$ ps, as shown in figure 7(b), correspond mostly to transition frequencies to levels with long vibrational periods (for example, $v = 227$ to $v = 233$ with $T_{\text{vib}} = 5.1$ ps to 6.3 ps).

Certain wavepacket components are filtered out to facilitate a shaping of the excited state wavepacket which is favourable for the dump step. This is illustrated for $\Delta t = 15.75$ ps in figure 8. The excited state wavepacket at $t = 15.75$ ps after the unshaped, figure 8(a), and optimized, figure 8(c), pump pulses is compared to the vibrational wavefunction of the ground state target level, figure 8(b). Optimal dump conditions are obtained when the wavepacket is

focused on the region where the target state wavefunction possesses its outermost maximum. The optimization leads to a removal of parts of the wavepacket in the inner region which would cause destructive interference in the dump process.

4. Conclusions and outlook

We have investigated to which extent the formation of ultracold molecules by pulsed photoassociation can be controlled using adaptive feedback control and shaped femtosecond laser pulses. For this purpose, we have set up a perturbative pulse shaper model and combined it with a genetic algorithm. This concept allows for a numerically efficient optimization with realistic conditions for the femtosecond laser pulse and the pulse shaper. Using the model for a pump-dump scheme, the population in a specific target level in the ground electronic state is optimized. A considerable enhancement factor of about 40% is achieved compared to highest population achieved with unshaped pulses, while keeping the pulse duration as short as possible. The maximum pump-dump enhancement in the perturbative, low-energy regime is determined by the Franck–Condon factors of the two electronic transitions. Significantly, larger enhancements may only be expected for high-intensity pulses beyond the perturbative regime, where Rabi cycling and dynamic Stark shifts occur.

The adaptive feedback optimization has shown that for different time delays between the pump and dump pulses, a maximum in the ground state molecule formation rate of similar height is achieved. This implies that the pump-dump delay represents an uncritical parameter as long as it is shorter than the spontaneous decay time in the sense that the optimization algorithm may find an optimal solution with a comparable target level population for arbitrary delay times. The analysis of the excited state wavepacket dynamics reveals that the shaped pulse induces a spatial focusing of the wavepacket on the Franck–Condon region of the dump pulse at the specified pump-dump delay. The pulse shaper can therefore greatly alter the dynamics of the wavepacket to optimize ground state molecule formation.

The model described in this work is advantageous compared to standard theoretical approaches such as the optimal control theory [39] in that it closely resembles the situation in experiments. Optimal control calculations generally converge faster than genetic algorithm optimizations, and extremely efficient pulses can be obtained [40]. However, these pulses are usually too complex to be directly implemented in an experiment [22, 23]. In this work, the optimized pulses are obtained in the frequency domain and are given in terms of the transmission coefficients and phase shifts of a pulse shaper. The optimization results can therefore directly be employed in experiments.

Future improvements of the presented calculations may follow several lines. To obtain absolute rates for molecule formation, a thermal average needs to be performed. This will be important to find pulse shapes for which association dominates over photodissociation of ultracold molecules [24, 28]. For the collision energies in a magneto-optical trap, such an average requires inclusion of partial waves with $l > 0$. Second, all relevant electronic states need to be incorporated in the model. In particular, resonant spin–orbit coupling is known to lead to perturbations in the excited state vibrational spectrum [33, 41] which might be important for ground state molecule formation [20]. Furthermore, it will be interesting to investigate the influence of the laser field polarization on ground state molecule formation, in particular, to find shaped pulses which excite specific molecular symmetries. Finally, higher order terms may be included in the perturbative derivation of the pulse shaper model to allow for investigation of the nonlinear excitation regime. Here, higher enhancement factors beyond the Franck–Condon regime may be expected. Based on the findings in this work, dedicated experiments on pulsed photoassociation of ultracold rubidium molecules are in progress.

Acknowledgments

References

[1] Hinds E A 1997 Testing time reversal symmetry using molecules *Phys. Scr.* **T70** 34

[2] Bartenstein M, Altmeyer A, Riedl S, Jochim S, Chin C, Hecker Denschlag J and Grimm R 2004 Crossover from a molecular Bose–Einstein condensate to a degenerate fermi gas *Phys. Rev. Lett.* **92** 120401

[3] DeMille D 2002 Quantum computation with trapped polar molecules *Phys. Rev. Lett.* **88** 067901

[4] Herbig J, Kraemer T, Mark M, Weber T, Chin C, Nägerl H-C and Grimm R 2003 *Science* **301** 1510

[5] Thorsheim H R, Weiner J and Julienne P S 1987 Laser induced photoassociation by spontaneous anti-Stokes scattering *Phys. Rev. Lett.* **58** 2420

[6] Lett P D, Helmerson K, Philips W D, Ratcliff L P, Rolston S L and Wagshul M E 1993 Spectroscopy of na2 by photoassociation of laser-cooled na *Phys. Rev. Lett.* **71** 2200

[7] Fioretti A, Comparat D, Crubellier A, Dulieu O and Masnou-Seeuws F 1998 Formation of cold cs2 through photoassociation *Phys. Rev. Lett.* **80** 4402

[8] McKenzie C *et al* 2002 *Phys. Rev. Lett.* **88** 120403

[9] Vanhaecke N, Lisdat C, T'Jampens B, Comparat D, Crubellier A and Pillet P 2004 Accurate asymptotic ground state potential curves of cs2 from two-colour photoassociation *Eur. Phys. J.* D **28** 351

[10] Ryu C, Du X, Yesilada E, Dudarev A M, Wan S, Niu Q and Heinzen D J 2005 *Preprint* cond-mat/0508201

[11] Sage J M, Sainis S, Bergeman T and DeMille D 2005 Optical production of ultracold polar molecules *Phys. Rev. Lett.* **94** 203001

[12] Machholm M, Giusti-Suzor A and Mies F 1994 Photoassociation of atoms in ultracold collisions probed by wave-packet dynamics *Phys. Rev. A* **50** 5025

[13] Kraft S D, Mudrich M, Staudt M, Lange J, Dulieu O, Wester R and Weidemüller M 2005 Saturation of cs2 photoassociation in an optical dipole trap *Phys. Rev. A* **71** 013417

[14] Judson R and Rabitz H 1992 Teaching lasers to control molecules *Phys. Rev. Lett.* **68** 1500

[15] Brixner T and Gerber G 2003 Quantum control of gas-phase and liquid-phase femtochemistry *Chem. Phys. Chem.* **4** 418

[16] Vala J, Dulieu O, Masnou-Seeuws F, Pillet P and Kosloff R 2000 Coherent control of cold-molecule formation through photoassociation using a chirped-pulsed-laser field *Phys. Rev. A* **63** 013412

[17] Luc-Koenig E, Kosloff R, Masnou-Seeuws F and Vatasescu M 2004 Photoassociation of cold atoms with chirped laser pulses: time-dependent calculations and analysis of the adiabatic transfer within a two-state model *Phys. Rev. A* **70** 033414

[18] Luc-Koenig E, Vatasescu M and Masnou-Seeuws F 2004 Optimizing the photoassociation of cold atoms by use of chirped laser pulses *Eur. Phys. J.* D **31** 239

[19] Koch C P, Luc-Koenig E and Masnou-Seeuws F 2006 Making ultracold molecules in a two colour pump-dump photoassociation scheme using chirped pulses *Phys. Rev. A* **73** 033408

[20] Koch C P, Kosloff R and Masnou-Seeuws F 2006 *Phys. Rev. A* **73** 043409

[21] Hornung T, Gordienko S, de Vivie-Riedle R and Verhaar B J 2002 Optimal convesion of an atomic to a molecular Bose–Einstein condensate *Phys. Rev. A* **66** 043607

[22] Hornung T, Motzkus M and de Vivie-Riedle R 2002 Teaching optimal control theory to distill robust pulses even under experimental constraints *Phys. Rev. A* **65** 021403

[23] Mančal T and May V 2002 Optimal control theory of ultrafast molecular dynamics: are the results of interest for the experiment? *Chem. Phys. Lett.* **362** 407

[24] Salzmann W *et al* 2006 Coherent control with shaped femtosecond laser pulses applied to ultracold molecules *Phys. Rev. A* **73** 023414

[25] Marvet U and Dantos M 1995 Femtosecond photoassociation spectroscopy: coherent bond formation *Chem. Phys. Lett.* **245** 393–9

[26] Fatemi F, Jones K M, Wang H, Walmsley I and Lett P D 2001 Dynamics of photoinduced collisions of cold atoms probed with picosecond laser pulses *Phys. Rev. A* **64** 033421

[27] Wright M J, Gensemer S D, Vala J, Kosloff R and Gould P L 2005 Control of ultracold collisions with frequency-chirped light *Phys. Rev. Lett.* **95** 063001

[28] Brown B L, Dicks A J and Walmsley I A 2006 Coherent control of ultracold molecule dynamics in a magneto-optical trap by use of chirped femtosecond laser pulses *Phys. Rev. Lett.* **96** 173002

[29] Park S, Suh S, Lee Y and Jeung G 2001 Theoretical study of the electronic states of the Rb2 molecule *J. Mol. Spectrosc.* **207** 129

[30] Marte A, Volz T, Schuster J, Dürr S, Rempe G, van Kempen E G M and Verhaar B J 2002 Feshbach resonances in rubidium 87: precision measurement and analysis *Phys. Rev. Lett.* **89** 283202

[31] Gutterres R F, Amiot C, Fioretti A, Gabbanini C, Mazzoni M and Dulieu O 2002 Determination of the ^{87}Rb 5p state dipole matrix element and radiative lifetime from the photoassociation spectroscopy of the $Rb_2 0_g^-(P_{3/2})$ long-range state *Phys. Rev.* A **66** 024502

[32] Spiegelmann F, Pavolini D and Daudey J-P 1989 Theoretical study of the excited states of the heavier alkali dimers: II. the Rb2 molecule *J. Phys. B: At. Mol. Opt. Phys.* **22** 2465

[33] Amiot C, Dulieu O and Vergès J 1999 Resolution of the apparent disorder of the Rb_2 $A^1\Sigma_u^1$ (0_u^+) and $b^3\Pi_u$ (0_u^+) spectra: a case of fully coupled electronic States *Phys. Rev. Lett.* **83** 2316

[34] Kokoouline V, Dulieu O, Kosloff R and Masnou-Seeuws F 1999 Mapped fourier methods for long-range molecules *J. Chem. Phys.* **110** 9865

[35] Willner K, Dulieu O and Masnou-Seeuws F 2004 Mapped grid methods for long-range molecules and cold collisions *J. Chem. Phys.* **120** 548

[36] Kosloff R 1988 Time-dependent quantum-mechanical methods for molecular dynamics *J. Phys. Chem.* **92** 2087

[37] de Araujo L and Walmsley I 2003 Analytic solution for quantum control of atomic and molecular wavepackets *J. Opt.* B **5** R27

[38] Wall M 2005 GAlib 2.4.6, Massachusetts Institute of Technology. http://lancet.mit.edu/ga

[39] Zhu W, Botina J and Rabitz H 1997 Rapidly convergent iteration methods for optimal control of population *J. Chem. Phys.* **108** 1953

[40] Koch C P, Palao J, Kosloff R and Masnou-Seeuws F 2004 Stabilization of ultracold molecules using optimal control theory *Phys. Rev.* A **70** 013402

[41] Jelassi H, Viaris de Lesegno B and Pruvost L 2006 *Phys. Rev.* A **73** 032501